AMERICAN SOCIETY FOR MICROBIOLOGY | Journal of Virology®

PATHOGENESIS AND IMMUNITY

CD8$^+$ T Cells and Macrophages Regulate Pathogenesis in a Mouse Model of Middle East Respiratory Syndrome

Christopher M. Coleman,[a] Jeanne M. Sisk,[a]* Gabor Halasz,[b] Jixin Zhong,[c] Sarah E. Beck,[c] Krystal L. Matthews,[a] Thiagarajan Venkataraman,[a] Sanjay Rajagopalan,[c] Christos A. Kyratsous,[b] Matthew B. Frieman[a]

Department of Microbiology and Immunology, University of Maryland School of Medicine, Baltimore, Maryland, USA[a]; Regeneron Pharmaceuticals, Tarrytown, New York, USA[b]; Department of Medicine, University of Maryland School of Medicine, Baltimore, Maryland, USA[c]

ABSTRACT Middle East respiratory syndrome coronavirus (MERS-CoV) is an important emerging pathogen that was first described in 2012. While the cell surface receptor for MERS-CoV has been identified as dipeptidyl peptidase 4 (DPP4), the mouse DPP4 homologue does not allow virus entry into cells. Therefore, development of mouse models of MERS-CoV has been hampered by the fact that MERS-CoV does not replicate in commonly available mouse strains. We have previously described a mouse model in which mDPP4 was replaced with hDPP4 such that hDPP4 is expressed under the endogenous mDPP4 promoter. In this study, we used this mouse model to analyze the host response to MERS-CoV infection using immunological assays and transcriptome analysis. Depletion of CD4$^+$ T cells, CD8$^+$ T cells, or macrophages has no effect on MERS-CoV replication in the lungs of infected mice. However, we found that depletion of CD8$^+$ T cells protects and depletion of macrophages exacerbates MERS-CoV-induced pathology and clinical symptoms of disease. Overall, we demonstrate an important role for the inflammatory response in regulating MERS-CoV pathogenesis *in vivo*.

IMPORTANCE The Middle East respiratory syndrome coronavirus (MERS-CoV) is a highly pathogenic respiratory virus that emerged from zoonotic sources in 2012. Human infections are still occurring throughout Saudi Arabia at a 38% case fatality rate, with the potential for worldwide spread via air travel. In this work, we identify the host response to the virus and identify inflammatory pathways and cell populations that are critical for protection from severe lung disease. By understanding the immune response to MERS-CoV we can develop targeted therapies to inhibit pathogenesis in the future.

KEYWORDS MERS-CoV, DPP4, mouse model, pathogenesis, MERS, coronavirus, immune response, viral pathogenesis

Middle East respiratory syndrome coronavirus (MERS-CoV) was first reported in the Kingdom of Saudi Arabia (KSA) in 2012 (1). As of 30 June 2016, there have been 1,769 confirmed MERS-CoV cases, with 630 deaths, a case fatality rate of around 36%. While the majority of MERS-CoV cases have been reported in the Middle East, a total of 27 countries have reported MERS-CoV cases. Outside the Middle East, MERS-CoV cases have involved mostly people who have traveled to the Middle East, including a recent outbreak in The Republic of Korea (2, 3), where a traveler returned to Seoul and initiated significant local human-to-human transmission.

In vitro analysis of MERS-CoV and immune cells has suggested that MERS-CoV interacts with and infects T cells and macrophages. The receptor for MERS-CoV was identified as dipeptidyl peptidase 4 (DPP4) (4). T cells express DPP4, and DPP4 activity

Received 13 September 2016 **Accepted** 18 October 2016

Accepted manuscript posted online 26 October 2016

Citation Coleman CM, Sisk JM, Halasz G, Zhong J, Beck SE, Matthews KL, Venkataraman T, Rajagopalan S, Kyratsous CA, Frieman MB. 2017. CD8$^+$ T cells and macrophages regulate pathogenesis in a mouse model of Middle East respiratory syndrome. J Virol 91:e01825-16. https://doi.org/10.1128/JVI.01825-16.

Editor Julie K. Pfeiffer, University of Texas Southwestern Medical Center

Address correspondence to Matthew B. Frieman, mfrieman@som.umaryland.edu.

* Present address: Jeanne M. Sisk, Department of Cell Biology, Johns Hopkins University School of Medicine, Baltimore, Maryland, USA.

is upregulated upon T cell activation (reviewed in reference 5). MERS-CoV is able to infect both $CD4^+$ and $CD8^+$ primary human T cells and, upon infection, induces T cell apoptosis *in vitro* (6). Interestingly, MERS-CoV RNA was detectable in splenic T cells in MERS-CoV-infected marmosets (6), suggesting that MERS-CoV infection of T cells may lead to the establishment of systemic viremia. Monocyte-derived macrophages express DPP4 (7) and can be infected by MERS-CoV *in vitro*, though whether MERS-CoV can productively replicate in macrophages is currently debated (7, 8). *In vitro* infection of human macrophages with MERS-CoV caused upregulation of cytokines and chemokines (7, 8). Zhou et al. showed significant infection-associated upregulation of tumor necrosis factor alpha (TNF-α), interleukin-6 (IL-6), gamma interferon (IFN-γ), CXCL10, CCL2, CCL3, CCL5, IL-8, and IL-12 and no upregulation of IFN-β (8), whereas Tynell et al. showed significant upregulation of IFN-β, IFN-λ1, CXCL10, and MxA and no upregulation of TNF-α expression (7). In both studies, there was a significant MERS-CoV-induced upregulation of CXCL10 expression in infected macrophages (7, 8), and CXCL10 is an IFN-γ-inducible T cell chemokine involved in $CD4^+$ recruitment and polarization to the Th1 and, possibly, Th17 subtypes (reviewed in reference 9).

There are few data on the pathological result of MERS-CoV infection in humans. However, the first, and so far only, autopsy of a fatal case of MERS-CoV infection has been recently published (10). Histopathology of the autopsied lungs revealed MERS-CoV replication in type II pneumocytes, with signs of pulmonary edema, diffuse alveolar damage with hyaline membrane formation, and thickening of the alveolar septa associated with a mixed lymphocyte infiltration (10). The authors did not find evidence of MERS-CoV replication in any extrapulmonary site, including the kidney or brain, and speculated that the kidney failure observed in this case was from general organ failure due to infection, for example, as a result of hypoperfusion or cytokine dysregulation (10).

MERS-CoV infection of rhesus macaques (11–13) or common marmosets (14) results in MERS-CoV replication and some signs of clinical disease, though neither recapitulates the severe disease seen in humans. Others have shown conflicting results for MERS-CoV-induced disease in marmosets (15). In addition, use of large nonhuman primates is expensive and not practical for large-scale screening of interventions *in vivo*. Therefore, development of a small-animal model for MERS-CoV is an important tool for studying the pathogenesis of MERS-CoV and to test and validate therapeutic strategies *in vivo*.

MERS-CoV is the second highly pathogenic coronavirus to emerge; the first was severe acute respiratory syndrome coronavirus (SARS-CoV). The human SARS-CoV strain SARS-CoV(Urbani) replicates efficiently in the lungs of wild-type BALB/c mice (16); therefore, a mouse model of SARS-CoV was developed by successful adaptation of SARS-CoV(Urbani) to mice by multiple passages (17). However, MERS-CoV is unable to replicate in the lungs of wild-type, or innately immune-deficient, commonly available mouse strains, limiting the possibility that *in vivo* virus passage could produce a mouse-adapted MERS-CoV strain (18). Mouse DPP4 (mDPP4) is not a functional receptor for MERS-CoV (19, 20) due to glycosylation of key amino acid residues in mDPP4 that inhibit binding of MERS-CoV spike (S) protein (21). To address this, attempts have been made to express human DPP4 (hDPP4) in mice, thereby making them susceptible to MERS-CoV entry. One such model involves the transduction of mouse lungs with an adenovirus expressing hDPP4 (Ad/hDPP4) (22). In mice transduced with Ad/hDPP4, MERS-CoV replicates efficiently and there are signs of lung inflammation by histology (22). This model was used to show that the type I interferon response, $CD8^+$ T cells, and neutralizing antibodies are required for efficient clearance of MERS-CoV (22). However, there are no visible signs of clinical disease, such as weight loss, and infection with this adenovirus does not result in stable expression of hDPP4 in the lungs of mice, with susceptibility to MERS-CoV diminishing at 22 days following adenovirus infection (22).

Others have generated transgenic mice expressing hDPP4 under a combined cytomegalovirus (CMV)/immediate early enhancer and the chicken β-actin promoter. In this mouse model, hDPP4 is expressed in almost every organ of the body (23), which does

not accurately reproduce the authentic tissue-specific distribution and level of expression of endogenously expressed mDPP4 (reviewed in reference 24). Accordingly, this model is characterized by robust MERS-CoV replication and rapid lethal disease characterized by inflammation in the lung and brain (23, 25). However, significant brain pathology has not been observed in MERS-CoV infection in humans (10).

Finally, a recent study has demonstrated that mice transgenic for hDPP4 under the epithelial-cell-specific promoters also support widespread MERS-CoV infection resulting in significant damage in the lungs and brain of infected mice (26). Although this model is improved relative to previously reported mouse models by limiting hDPP4 expression to epithelial cells, this is not coincident with the levels of expression and cell types in which endogenous mDPP4 is found.

All three models of MERS-CoV infection in mice (22, 25, 26) have robust replication of MERS-CoV and, as such, have utility as a vehicle for testing of novel therapeutics or vaccines that inhibit MERS-CoV replication (25, 26). However, they provide limited information about the natural pathogenesis of MERS-CoV infection *in vivo* (25).

We have recently shown that a humanized knock-in mouse expressing hDPP4 in place of mDPP4 has detectable MERS-CoV replication with histological signs of MERS disease, and we used it to test the efficacy of a novel MERS-CoV monoclonal antibody therapeutic. This limited-duration study, up to 4 days postinfection, did not demonstrate significant clinical signs of MERS-CoV infection, e.g., weight loss (27). In this study, we describe and characterize this novel mouse model for MERS-CoV infection in more detail. We find that from 5 to 7 days postinfection, MERS-CoV-infected mice display significant signs of clinical disease, including weight loss, ruffled fur, and labored breathing as well as significantly increased lung damage and inflammation. Analysis of lung inflammation in MERS-CoV-infected mice revealed alterations in the chemokine and cytokine response and leukocyte infiltration consistent with T cell- and macrophage-mediated responses. Transcriptome profiling corroborates these observations and suggests that there is also fibrotic gene upregulation, damage to the lung endothelium, and depletion of B cells in MERS-CoV-infected lungs. Using inflammatory cell depletion experiments, we further conclude that $CD8^+$ T cells exacerbate severe MERS-CoV lung disease while macrophages play a role in suppressing MERS-CoV-induced lung disease.

RESULTS

hDPP4 tissue and immune cell distribution is the same as endogenous mDPP4 tissue distribution in C57B6/hDPP4 mice. When developing a mouse model expressing the human virus receptor, a major concern is ensuring correct tissue distribution of the protein. Endogenous DPP4 expression is not restricted to the lungs and also has a distinct tissue distribution, with some organs expressing higher levels than others (reviewed in reference 24). By maintaining the mDPP4 gene promoter and the 3′ untranslated region (UTR) to control hDPP4 (27), we aimed to achieve a model in which hDPP4 matched the tissue distribution and expression levels observed for endogenous mDPP4. To test this, we compared hDPP4 mRNA expression to mDPP4 mRNA expression in a range of organs and in blood.

Using genotype-confirmed $hDPP4^{-/-}$, $hDPP4^{+/-}$, and $hDPP4^{+/+}$ mice, we assessed the expression levels of both mDPP4 and hDPP4 in mouse organs (Fig. 1A). The levels of hDPP4 in both $hDPP4^{+/-}$ and $hDPP4^{+/+}$ mice are comparable to those of mDPP4 in $hDPP4^{-/-}$ or $hDPP4^{+/-}$ mice in seven of the eight tissues assayed ($P > 0.05$) (Fig. 1A). The one significant discrepancy was in the kidney, where hDPP4 expression in $hDPP4^{+/-}$ and $hDPP4^{+/+}$ mice was significantly higher than mDPP4 expression in $hDPP4^{-/-}$ or $hDPP4^{+/-}$ mice; for example, hDPP4 in $hDPP4^{+/-}$ compared to mDPP4 in $hDPP4^{-/-}$; $P < 0.001$) (Fig. 1A). We observed no significant difference in mDPP4 distribution in $hDPP4^{+/-}$ mice compared to $hDPP4^{-/-}$ mice in all organs ($P > 0.05$) (Fig. 1A), suggesting that the replacement of mDPP4 with hDPP4 on one chromosome does not significantly affect endogenous mDPP4 expression.

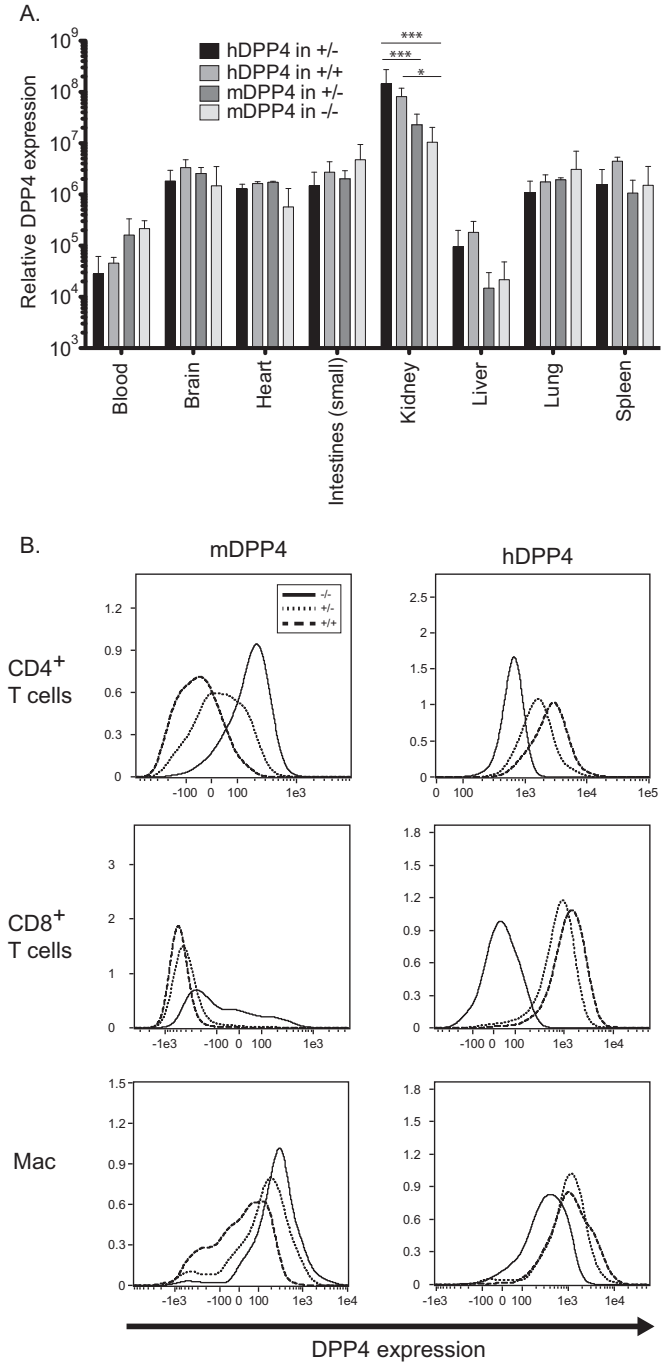

FIG 1 mDPP4 and hDPP4 expression in organs and immune cells of C57B6/hDPP4 mice. (A) Organs from wild-type C57B6 mice (hDPP4$^{-/-}$), C57B6/hDPP4$^{+/-}$, and C57B6/hDPP4$^{+/+}$ mice were removed and probed for mDPP4 or hDPP4 mRNA expression by reverse transcription (RT)-PCR. mDPP4 expression in C57B6/hDPP4$^{+/+}$ mice and hDPP4 expression in wild-type mice were used as baseline expression samples. Data shown are means ± SEM of samples from 2 mice. ***, $P < 0.001$; *, $P < 0.05$. (B) Splenocytes from wild-type C57B6 mice (hDPP4$^{-/-}$), C57B6/hDPP4$^{+/-}$, and C57B6/hDPP4$^{+/+}$ mice were stained for mDPP4 and hDPP4. Cells were identified as CD4$^+$ T cells, CD8$^+$ T cells, or macrophages (Mac) and assessed for DPP4 expression. Three mice from each group were used, and representative flow cytometry histograms are shown. Solid line, hDPP4$^{-/-}$; dotted line, hDPP4$^{+/-}$; dashed line, hDPP4$^{+/+}$.

We next assessed DPP4 expression on CD4$^+$ T cells, CD8$^+$ T cells, and macrophages (Fig. 1B). As expected, in all cases, mDPP4 expression was detectable on cells isolated from hDPP4$^{-/-}$ mice (Fig. 1B, first column, solid lines), and hDPP4 expression was detectable on hDPP4$^{+/+}$ mice (Fig. 1B, second column, dashed lines). While it is difficult

to quantifiably compare mDPP4 expression to that of hDPP4 due to different antibody affinities and fluorophores, there were detectable levels of mDPP4 and hDPP4 on hDPP4$^{+/-}$ mice (Fig. 1B, spotted lines). These data suggest that CD4$^+$ T cells, CD8$^+$ T cells, and macrophages from hDPP4$^{+/-}$ mice express both mDPP4 and hDPP4.

These data show that the hDPP4$^{+/-}$ and hDPP4$^{+/+}$ mice do not have significantly different expression of hDPP4 compared to endogenous mDPP4, in terms of both tissue distribution and expression levels, although hDPP4 appears to be more highly expressed than mDPP4 in the kidney.

hDPP4-expressing mice infected with MERS-CoV by intranasal inoculation display clinical signs of disease in a dose-dependent manner. We have previously shown that MERS-CoV infection in our C57B6 hDPP4-expressing mouse does not result in significant weight loss up to 4 days postinfection (27). To determine if hDPP4-expressing mice were susceptible to MERS-CoV disease at higher MERS-CoV doses and over a longer time course, we infected mice with 2.5×10^2, 2.5×10^3, or 2.5×10^4 PFU of MERS-CoV(Jordan) and monitored weight loss and clinical symptoms up to 21 days postinfection.

For the first 4 days of infection, there was no significant weight loss or clinical symptoms observed in any of the groups (Fig. 2A). However, starting from day 5 postinfection, mice infected with 2.5×10^4 PFU MERS-CoV(Jordan) lost significant weight, resulting in a $\geq$20% weight loss by day 7 postinfection in all mice (Fig. 2A, diamonds). They also displayed progressively worsening clinical signs of disease from day 5 postinfection, such as ruffled fur, lethargy, and hunched bearing. Mice infected with an intermediate dose of 2.5×10^3 PFU MERS-CoV(Jordan) lost 10% of their starting body weight by day 7 postinfection but, interestingly, regained 5% of starting body weight by day 8 and remained at $\geq$100% of starting body weight for the remainder of the time course from day 9 postinfection (Fig. 2A, triangles). These mice displayed no other visible signs of disease at any other time point. Mock-infected mice (Fig. 2A, circles) or mice infected with a low dose of 2.5×10^2 PFU MERS-CoV(Jordan) remained at $\geq$100% of their starting body weight for the entire time course (Fig. 2A, squares) and showed no visible signs of disease.

These data demonstrate that we have developed a useful model of MERS-CoV infection in which we can observe 3 distinct disease phenotypes based on the MERS-CoV inoculum: a lethal dose of MERS-CoV infection in mice (2.5×10^4 PFU/mouse), a dose at which mice show some symptoms but recover (2.5×10^3 PFU/mouse), and a dose at which there are no clinical symptoms of disease (2.5×10^2 PFU/mouse).

MERS-CoV replicates efficiently in lungs of hDPP4-expressing mice. We have previously shown that MERS-CoV titers and RNA were detectable in the lungs of MERS-CoV-infected mice up to 4 days postinfection (27). To extend these data and to confirm that mice infected with 2.5×10^2, 2.5×10^3, or 2.5×10^4 PFU were productively infected with MERS-CoV, we assessed MERS-CoV titers and RNA levels over a longer time course. As the mice infected with 2.5×10^4 PFU had all dropped below 80% of their starting body weight at 7 days postinfection and had to be sacrificed per IACUC regulations, there were no mice in this group for analysis at days 14 and 21 postinfection (Fig. 2B, C, and D, marked N/A). MERS-CoV titer was assayed by plaque assay on Vero cells, and MERS-CoV genomic RNA and mRNA levels were assayed by a TaqMan quantitative real-time PCR (qPCR) assay. Genomic RNA levels report on the amount of viral genome detected in the lungs, while the mRNA TaqMan primers detect only replicating virus by using a MERS-CoV Leader-specific primer as the 5′ primer. The mRNA primers report the presence of mRNAs that are found only when MERS-CoV is replicating in cells.

At 2 days postinfection, significant levels of infectious MERS-CoV could be detected in mice infected with all 3 doses of MERS-CoV (Fig. 2B). The levels of observed MERS-CoV are dependent upon the inoculated dose, as mice infected with 2.5×10^2 PFU MERS-CoV had a mean of 3.09×10^4 PFU/g MERS-CoV, mice infected with 2.5×10^3 PFU MERS-CoV had a mean of 1.25×10^5 PFU/g MERS-CoV, and mice infected with

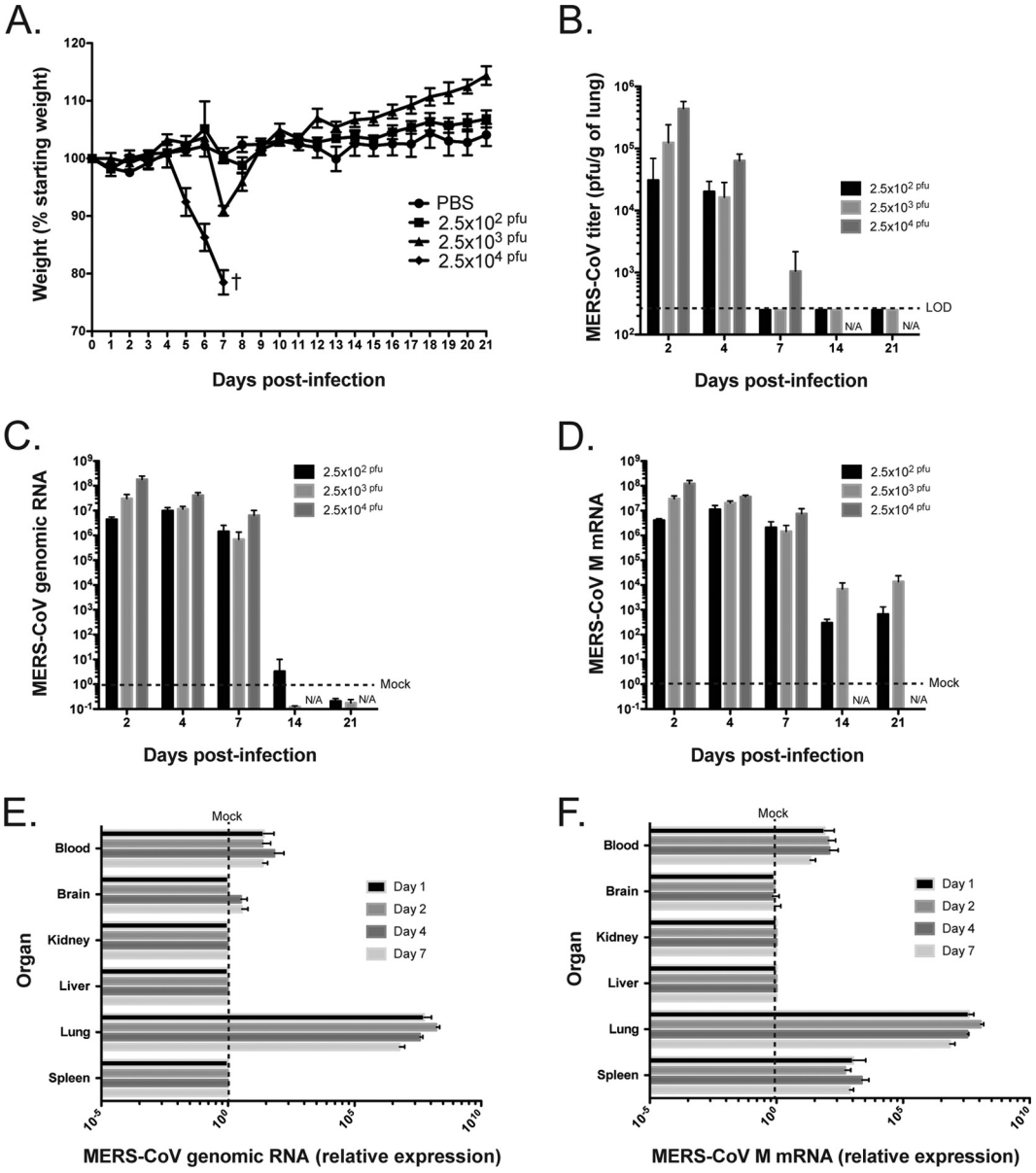

FIG 2 Characterization of MERS-CoV replication and disease in C57B6/hDPP4 mice. C57B6/hDPP4 mice were infected with 2.5×10^2, 2.5×10^3, or 2.5×10^4 PFU MERS-CoV(Jordan) and assessed for signs of disease and MERS-CoV replication. (A) MERS-CoV-induced weight loss was monitored up to 21 days postinfection. (B to D) MERS-CoV titers in the lung (B), MERS-CoV genomic RNA expression in the lung (C), and MERS-CoV M RNA expression in the lung (D) were assessed at 2, 4, 7, 14, and 21 days postinfection. N/A, not applicable (all mice infected with 2.5×10^4 PFU dropped below 80% of their starting body weight at 7 days postinfection and had to be sacrificed per IACUC regulations). (E and F) To assess the spread of MERS-CoV, MERS-CoV genomic RNA (E) and M mRNA (F) were also assessed in the blood, brain, kidney, liver, and spleen of mice infected with 2.5×10^4 PFU MERS-CoV(Jordan). Data in panel A represent means ± SEM of results for 5 to 30 mice, with 5 mice per sacrifice time point as shown in panels B to D, per infection. Data in panels B to F are means ± SEM of results from 5 mice. LOD, limit of detection.

2.5×10^4 PFU MERS-CoV had a mean of 2.05×10^5 PFU/g MERS-CoV (Fig. 2B). We also observed significant MERS-CoV genomic RNA (Fig. 2C) and mRNA (Fig. 2D) at day 2 postinfection, which again correlated with the inoculated dose of MERS-CoV.

At day 4 postinfection, the levels of infectious MERS-CoV detected in lungs of mice infected with 2.5×10^3 or 2.5×10^4 PFU MERS-CoV dropped 5- to 10-fold compared to levels at day 2 postinfection (Fig. 2B), whereas levels of infectious MERS-CoV detected in lungs of mice infected with 2.5×10^2 PFU MERS-CoV remained at the levels observed at day 2 postinfection (2.04×10^4 mean PFU/g [Fig. 2B]). This is consistent

with the levels of MERS-CoV genomic RNA (Fig. 2C) and M mRNA (Fig. 2D) at day 4 postinfection, when the 2.5×10^2 PFU-infected mice showed an increase in MERS-CoV RNA, while mice infected with either 2.5×10^3 or 2.5×10^4 PFU MERS-CoV showed a decrease in MERS-CoV RNA levels.

At 7 days postinfection, there was no detectable MERS-CoV titer in the lungs of mice infected with the low or intermediate dose of MERS-CoV and a mean of only 1.05×10^3 PFU/g of MERS-CoV in the lungs of mice infected with the high dose of MERS-CoV (Fig. 2B). However, high levels of MERS-CoV genomic RNA (Fig. 2C) and M RNA (Fig. 2D) were detected in all infected groups, though we did observe a dose-dependent decrease in MERS-CoV RNA levels at day 7 postinfection compared to day 4 postinfection for all doses (Fig. 2C and D). We suspect both that the TaqMan assay to detect RNA is more sensitive than plaque assay and that the viral RNA may be stable longer in the lungs than live virus. Using these assays, neither MERS-CoV (Fig. 2B) nor MERS-CoV genomic RNA (Fig. 2C) was detected at days 14 or 21 postinfection in mice infected with 2.5×10^2 or 2.5×10^3 PFU MERS-CoV except for the 2.5×10^2 group at day 14, in which we observe genomic RNA just above background levels. Low levels of MERS-CoV M mRNA, 3 log lower than the day 7 time point, were detectable at days 14 and 21 postinfection in mice infected with either 2.5×10^2 or 2.5×10^3 MERS-CoV (Fig. 2D).

These data indicate that mice infected with all three doses of MERS-CoV had a productive MERS-CoV infection in the lungs and that the kinetics of infection was dose dependent.

MERS-CoV does not spread to the brain, liver, or kidney but can be detected in the blood of hDPP4-expressing mice infected with 2.5×10^4 PFU MERS-CoV. To determine if mice expressing hDPP4 under the endogenous mouse promoter displayed a disseminated pattern of MERS-CoV infection, we measured the levels of MERS-CoV RNA in the blood, brain, liver, kidney, and spleen of mice intranasally infected with 2.5×10^4 PFU MERS-CoV(Jordan) (Fig. 2E and F), as these mice had the highest levels of MERS-CoV replication in the lungs. We were unable to detect expression of either MERS-CoV genomic RNA or M mRNA in the brain, liver, or kidney of mice infected by MERS-CoV compared to mock-infected controls (Fig. 2E and F). On the other hand, MERS-CoV genomic RNA and M mRNA were detectable in the blood of MERS-CoV-infected mice throughout the time course of infection (Fig. 2F). In addition, we observed detectable amounts of MERS-CoV M mRNA, but not genomic RNA, in the spleen of the MERS-CoV-infected mice at all postinfection time points (Fig. 2F). While MERS-CoV RNA was detectable in blood and spleen, both genomic and M mRNA levels in these tissues were many orders of magnitude lower than the levels measured in the lung.

These data suggest that MERS-CoV is present at a low level into the bloodstream of infected mice, either as free virions in the plasma or by infection of DPP4-expressing circulating leukocytes, which may traffic to the spleen. These data also demonstrate that MERS-CoV does not infect the brain, liver, or kidney over the time course of fatal infection in our C57B6/hDPP4 mice. Taken together, these data suggest that mortality of MERS-CoV in C57B6/hDPP4 mice is caused by the primary lung infection.

Infection with MERS-CoV results in significant lung pathology characterized by vascular cuffing and lymphocyte influx. Mice infected with mouse-adapted SARS-CoV display distinct pathological effects within the lungs, characterized by inflammatory cell infiltration and epithelial cell destruction (17). We have previously described that lungs of mice expressing hDPP4 infected with MERS-CoV show significant interstitial inflammation with perivascular cuffing and extensive alveolar septal thickening (27), but we did not observe any weight loss at day 4 postinfection. Based on the dose-dependent clinical disease and weight loss that we observed in the current study, we sought to further characterize the pathological effects of MERS-CoV. Examples of the types of pathology observed in MERS-CoV-infected mice are shown in Fig. 3.

Mice infected with 2.5×10^2 PFU, 2.5×10^3 PFU, or 2.5×10^4 PFU MERS-CoV(Jordan) displayed various levels of lymphocytic perivascular inflammation, macrophage infiltration, pleuritis, and epithelial necrosis (Tables 1, 2, and 3). In the $2.5 \times$

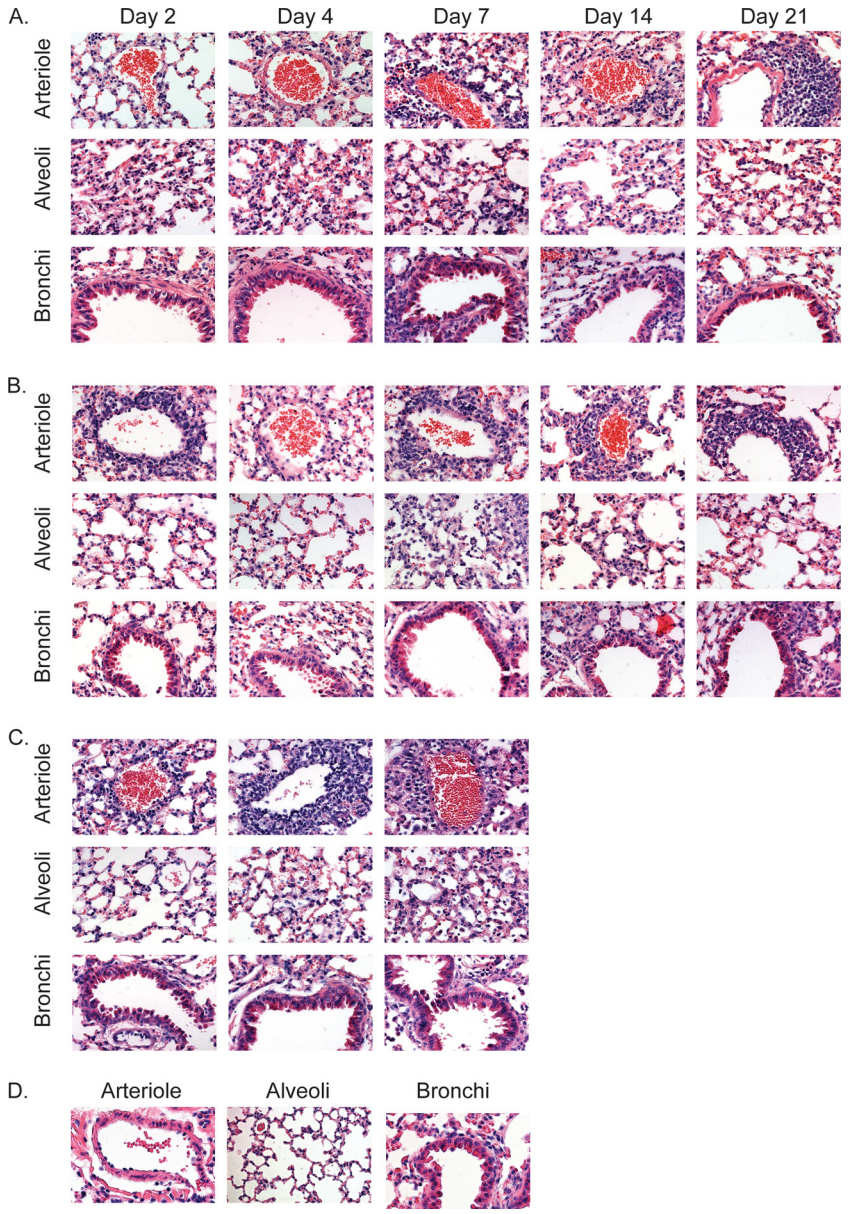

FIG 3 Histology of lungs of C57B6/hDPP4 mice infected with MERS-CoV. Images from lung sections of C57B6/hDPP4 mice infected with 2.5×10^2 (A), 2.5×10^3 (B), or 2.5×10^4 (C) PFU of MERS-CoV(Jordan). (D) PBS-inoculated mice. Pictures of blood vessels (arterioles), alveoli, and bronchioles were taken for comparative analysis of inflammatory structures in the lungs during infection.

10^2-PFU MERS-CoV-infected mice, lymphocytic perivascular inflammation was still evident through day 21 postinfection while all other inflammatory parameters were resolved by day 14 postinfection (Table 1). On the other hand, in mice infected with 2.5×10^3 PFU MERS-CoV, all pathological signs of disease, including lymphocytic perivascular inflammation, were resolved by day 14 postinfection (Table 2). In mice infected with 2.5×10^4 PFU MERS-CoV, no inflammatory resolution was observed by day 7 postinfection, and in addition, there was evidence of moderate edema (Table 3).

Overall, these data suggest that MERS-CoV infection of hDPP4-expressing mice causes a dose-dependent inflammatory disease characterized by predominantly perivascular inflammation that consists of mostly macrophages and lymphocytes.

Transcriptome analysis of MERS-CoV-infected B6/hDPP4 mice demonstrates recruitment and activation of T cells and macrophages. Compared to the lower

TABLE 1 Pathology scores of lungs of mice infected with 2.5×10^2 PFU MERS-CoV(Jordan)[a]

	Mean disease score at dpi:				
Pathological sign	**2**	**4**	**7**	**14**	**21**
Overall inflammation	+	+	++	++	++
Bronchiolar inflammation	+	+	+	+	+
Perivascular inflammation	+	++	++	++	++
Edema	+	+	+	+	+
Eosinophils	+	+	+	+	+
Neutrophils	+	+	+	+	+
Macrophages	+	+	++	+	+
Lymphocytes	+	++	++	++	++
Pleuritis	+	+	++	+	+
Epithelial necrosis	+	+	++	+	+

[a]Lung sections from 5 MERS-CoV-infected mice per group were scored for pathological signs of disease on a scale of 0 to 5, and scores were averaged and rounded to the nearest whole number: +, 0 or 1; ++, 2 or 3; +++, 4 or 5; dpi, days postinfection.

doses tested, mice infected with 2.5×10^4 PFU MERS-CoV display the most severe MERS-CoV infection phenotype; therefore, we decided to characterize the inflammatory response in C57B6/hDPP4 mice infected with 2.5×10^4 PFU of MERS-CoV by transcriptome analysis of infected lungs. Lungs from C57B6/hDPP4 mice infected with 2.5×10^4 PFU MERS-CoV(Jordan) were analyzed by strand-specific RNA sequencing (RNA-Seq) for transcriptional changes compared to lungs from mock-infected mice. We found a substantially altered lung transcriptional profile that correlates with the histological data in Fig. 2.

At day 2 postinfection, we detected 1,900 genes with expression altered by at least 50% compared to mock-infected controls. By 4 days postinfection, 2,484 genes were differentially regulated, and by day 7 postinfection, 5,536 genes, or about one-quarter of the mouse genome, was perturbed. The most pronounced changes were observed in genes associated with the inflammatory response. As early as day 2 postinfection, multiple cytokines and chemokines associated with both Th1 and Th2 responses were dramatically upregulated in infected lungs compared to mock-infected controls, including Cxcl11 (252-fold increase), Cxcl10 (222-fold), and others (Ccl7, Cxcl9, Ccl12, Ccl2) (Fig. 4B; see also Table S1 in the supplemental material for a full list of gene changes). All these genes retain their markedly elevated expression levels through day 7 postinfection, when the mice had to be sacrificed due to $\geq$20% weight loss.

Unsupervised hierarchical clustering allowed for further classification of these gene changes. The set of genes perturbed at day 7 postinfection compared to mock-infected controls fell roughly into four categories (Fig. 4A). The cytokines noted above clustered together into one group (shown in red on the heatmap in Fig. 4A). Members of this

TABLE 2 Pathology scores of lungs of mice infected with 2.5×10^3 PFU MERS-CoV(Jordan)[a]

	Mean disease score at dpi:				
Pathological sign	**2**	**4**	**7**	**14**	**21**
Overall inflammation	++	++	++	+	+
Bronchiolar inflammation	+	+	+	+	+
Perivascular inflammation	+	++	++	+	+
Edema	+	+	+	+	+
Eosinophils	+	+	+	+	+
Neutrophils	+	+	+	+	+
Macrophages	+	++	++	+	+
Lymphocytes	++	++	++	+	+
Pleuritis	+	++	+	+	+
Epithelial necrosis	+	+	++	+	+

[a]Lung sections from 5 MERS-CoV-infected mice per group were scored for pathological signs of disease on a scale of 0 to 5, and scores were averaged and rounded to the nearest whole number: +, 0 or 1; ++, 2 or 3; +++, 4 or 5; dpi, days postinfection.

TABLE 3 Pathology scores of lungs of mice infected with 2.5×10^4 PFU MERS-CoV(Jordan)[a]

Pathological sign	Mean disease score at dpi:		
	2	4	7
Overall inflammation	++	++	++
Bronchiolar inflammation	+	+	+
Perivascular inflammation	++	++	++
Edema	+	+	++
Eosinophils	+	+	+
Neutrophils	+	+	++
Macrophages	+	+	++
Lymphocytes	++	++	++
Pleuritis	+	+	+
Epithelial necrosis	+	+	+

[a]Lung sections from 5 MERS-CoV-infected mice per group were scored for pathological signs of disease on a scale of 0 to 5, and scores were averaged and rounded to the nearest whole number: +, 0 or 1; ++, 2 or 3; +++, 4 or 5; dpi, days postinfection.

group showed sharply elevated expression by day 2 postinfection (the first time point assayed) and continued to be overexpressed throughout the time course. A large number of cytokines, interleukins, and interferons follow this pattern of expression; for example, gamma interferon was 40-fold upregulated compared to mock-infected controls by day 7 postinfection, and Timp1, Serpine1, Thbs1, and other genes associated with fibrosis were also significantly upregulated (Fig. 4B).

The second cluster (Fig. 4A, orange) shows a more gradual pattern, with expression increasing over the time course of infection or only at day 7. Many genes in this category were associated with cell adhesion and wound-healing functions. Thus, while genes in the red group signify the acute phase of fibrosis, those in this orange group (e.g., Col3a1 and other collagens, Tgfb1) were associated with more-established disease. Proteasome components are also highly enriched in this group, with expression peaking at day 7 postinfection (Fig. 4B, brown lines).

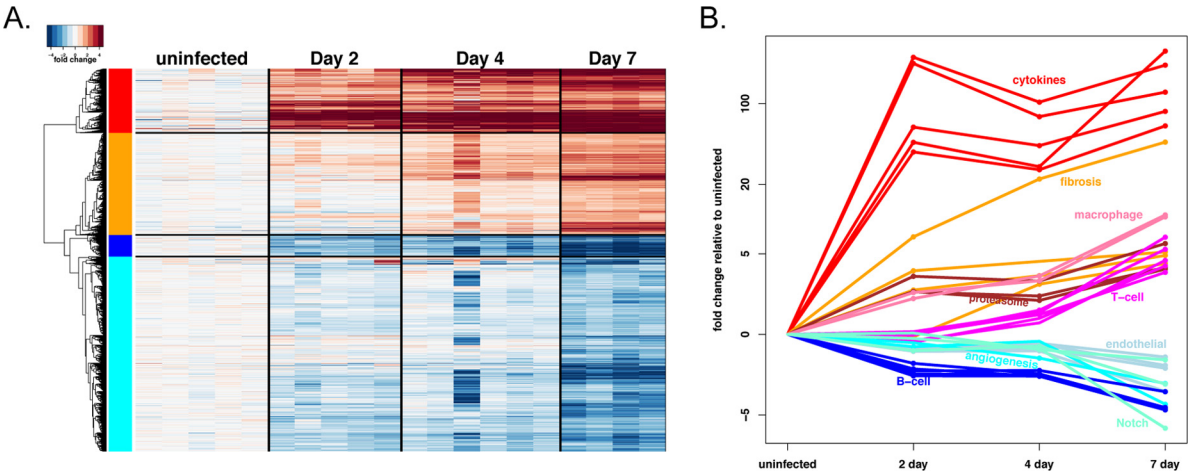

FIG 4 Gene expression changes in lungs of C57B6/hDPP4 mice infected with MERS-CoV. After infection with 2.5×10^4 PFU MERS-CoV(Jordan), C57B6/hDPP4 mouse lungs were harvested at 2, 4, and 7 days postinfection and profiled by RNA-Seq. Lungs from mock-infected mice were used as controls. (A) Heatmap showing gene expression changes across samples. Each column represents a mouse sample, while each row represents 1 of 5,536 genes whose expression is significantly altered between day 7 postinfection mice and controls. RPKM expression values for each gene are plotted as $\log_2$ ratios to the median in the mock-infected group. Unsupervised hierarchical clustering on these ratios yields four functionally relevant subgroups, indicated by the four colors in the left panel. (B) Expression of representative genes over the time course of infection. Values are fold changes (mean for infected mice at the indicated time point divided by the mean for the mock-infected mice). Dark circles indicate significantly perturbed gene changes ($P < 0.01$). Representative genes are as follows, listed for each group in order of diminishing fold change at day 7: cytokine group, Cxcl9, Cxcl11, Cxcl10, Ccl7, Ccl2; Fibrosis group, Timp1, Mmp13, Serpine1, Col1a1; macrophage group, C1qa, C1qc; T-cell group, Cd8a, Cd3e, Cd3g, Themis, Cd4; proteasome group, Psmb8, Psmb9, Psme1; endothelial group, Robo4, Pecam1, Egfl7, Tie1; angiogenesis group, Vegfa, Dll4. B-cell: Cd79b, Ms4a1, Cd19, Pax5, Cd79a; Notch group, Hes1, Nrarp, Hey1.

The largest category derived from unsupervised clustering (Fig. 4A, cyan) showed the inverse pattern, with expression diminishing toward the later time points of infection. Functional groups enriched for genes within this category included angiogenesis (Vegfa, Dll4), the Notch pathway (Hey1, Hes1, and Nrarp), and endothelial markers (Robo4, Pecam1) (cyan, aqua, and light blue lines in Fig. 4B).

The upregulated cytokines suggest T cell and macrophage recruitment upon infection with MERS-CoV. For example, both Cxcl11 and Cxcl10 are chemokines that promote T cell migration. To investigate further, we used a panel of genes showing cell-type-specific expression, as derived by the Immgen consortium (28), to assess immune subtype changes. We observed a sudden increase in T cell markers such as Cd3e and Themis by day 7, though not before (Fig. 4B, magenta lines). Thus, there is a pronounced delay between elevated cytokine expression and recruitment of T cells. Genes associated with macrophage proliferation were significantly upregulated upon MERS-CoV infection, with C1qc and C1qa levels increasing 2-fold by day 2 compared to mock-infected controls and reaching over 6-fold by day 7 (Fig. 4B, pale red lines). In contrast, there was significant downregulation of B cell markers (Cd19, Cd79a) at day 2 postinfection, compared to mock-infected controls, with continued reduction over the remainder of the time course (Fig. 4B, dark blue lines). B cell-associated genes are the only cluster whose members showed diminishing expression levels over the entire time course of MERS-CoV infection (Fig. 4B, blue). The dendritic cell marker Fscn1 was modestly upregulated at days 4 and 7 postinfection, while NK cell markers (Itga2, Ncr1) were unchanged.

Lastly, we asked whether the set of gene changes observed in our experiment resembled any in the public domain. To this end, we used NextBio, which compares pairs of gene signatures based on a running Fisher test-based algorithm (29). From among the 18,125 experiments in NextBio's database of public studies, the top four experiments matching the gene signature obtained from MERS-CoV-infected lungs at day 7 were all analogous to experiments in which SARS-CoV-infected mouse lungs (see Table S2 in the supplemental material). These results confirm the shared biology underpinning the host response to coronavirus infection. Our MERS-CoV infection signature also strongly matched other viral infections of the lung, for example, influenza virus H1N1 and bleomycin-treated lungs (Table S2).

Lungs of hDPP4 mice infected with MERS-CoV are infiltrated with macrophages, neutrophils, and both CD4$^+$ and CD8$^+$ T cells over the course of infection. To validate the results of the RNA-Seq analysis and histological observations, we next quantified the specific leukocyte populations present in the lungs of hDPP4-expressing mice infected with 2.5×10^4 PFU MERS-CoV over the time course of infection. We used flow cytometry to specifically identify subsets of lymphocytes (B cells, NK cells, CD4$^+$ T cells, and CD8$^+$ T cells), antigen-presenting cells (APCs; dendritic cells [DCs] and macrophages), and granulocytes (basophils, eosinophils, and neutrophils). At 2 days postinfection, there is no significant difference in lung leukocyte populations in MERS-CoV-infected mice compared to mock-infected controls ($P > 0.05$ for all cell types) (Fig. 5A). However, by 4 days postinfection, macrophage levels were significantly increased (6- $\pm$ 2.8-fold higher; $P < 0.001$) (Fig. 5B) and remained significantly elevated at day 7 postinfection ($P < 0.001$) (Fig. 5C). Neutrophils also increased at day 4 (3.2- $\pm$ 0.8-fold; $P < 0.05$), although there was no significant difference in neutrophil numbers compared to mock-infected controls at day 7 postinfection ($P > 0.05$) (Fig. 5C). Both CD4$^+$ and CD8$^+$ T cell numbers significantly increased 4-fold at day 7 postinfection compared to mock-infected controls ($P < 0.001$ in both cases) (Fig. 5C). Numbers of B cells, NK cells, DCs, basophils, and eosinophils in the lungs were not significantly affected by MERS-CoV infection at any time point compared to mock-infected controls (Fig. 5A, B, and C) ($P > 0.05$ in all cases). When data are plotted respective to the mock-infected controls (Fig. 5D), clear increases of CD4$^+$ T cells, CD8$^+$ T cells, and macrophages can be observed over the time course of MERS-CoV lung infection.

These data suggest that MERS-CoV infection induces the influx of macrophages, neutrophils, and CD4$^+$ and CD8$^+$ T cells into the lungs of infected mice in a time-

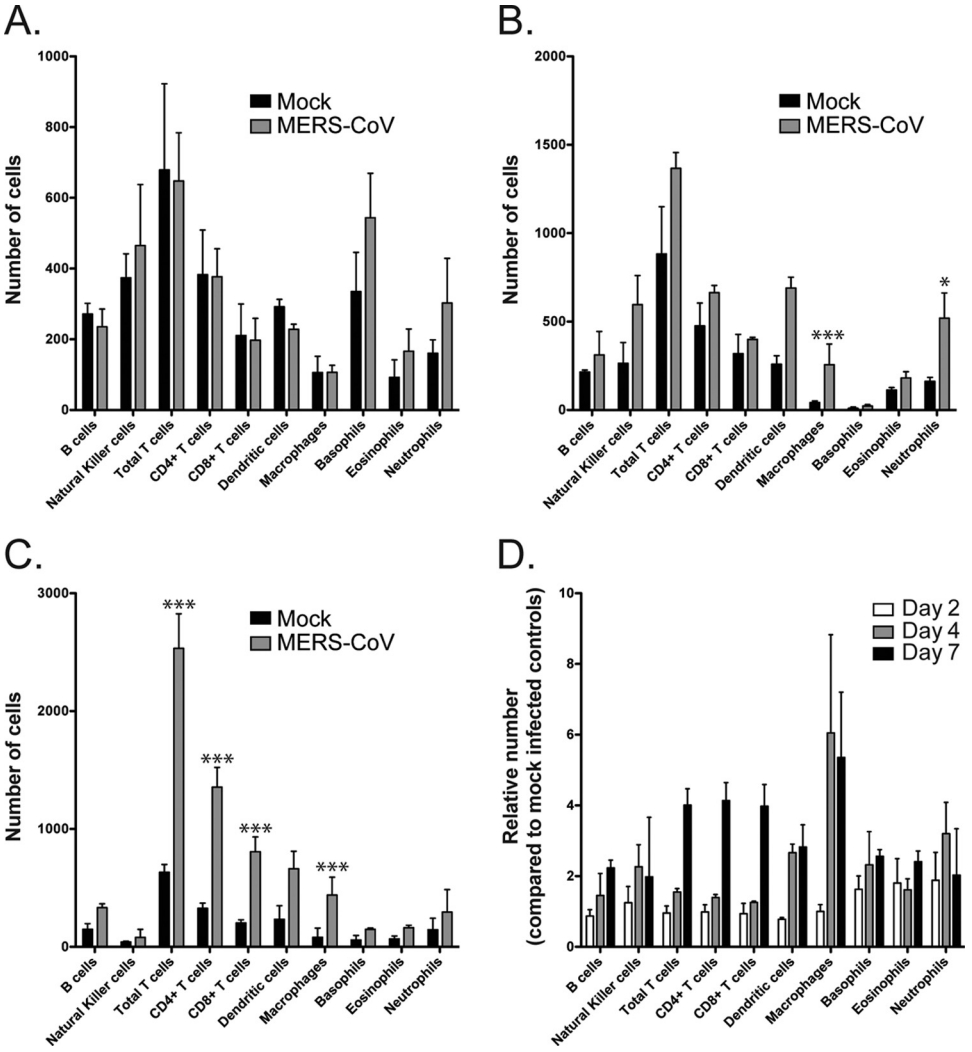

FIG 5 Infiltration of CD4$^+$ T cells, CD8$^+$ T cells, macrophages, and neutrophils into the lungs of MERS-CoV-infected C57B6/hDPP4 mice. (A to C) C57B6/hDPP4 mice were infected with 2.5×10^4 PFU MERS-CoV (Jordan) and assessed for leukocyte infiltration at day 2 postinfection (A), day 4 postinfection (B), and day 7 postinfection (C). (D) Compared to mock-infected controls, significant peaks of CD4$^+$ T cells, CD8$^+$ T cells, and macrophages can be observed over the time course. Data shown are means $\pm$ standard deviations (SD) for samples from 3 mice per time point.

dependent manner. Neutrophils infiltrate up to 4 days postinfection but then return to background levels for the remainder of the infection. CD4$^+$ and CD8$^+$ T cells infiltrate after day 4 postinfection and reach very high levels by 7 days postinfection, whereas macrophages infiltrate the lungs of infected mice from day 4 postinfection and are still at high levels at 7 days postinfection. The infiltration of macrophages and T cells shows remarkable concordance with the transcriptome profiling observations, both in the magnitude and kinetics of the changes.

Depletion of CD4$^+$ T cells has no effect on MERS-CoV infection or pathogenesis, whereas depletion of CD8$^+$ T cells reduces weight loss in MERS-CoV-infected C57B6/hDPP4 mice. Taken together, the histology, flow cytometry, RNA-Seq, and cytokine and chemokine data suggest that MERS-CoV disease in mice is characterized by a large influx of T cells into the lungs of infected mice. However, as both CD4$^+$ and CD8$^+$ T cells are present in higher numbers in MERS-CoV-infected mice, the relative contributions of each cell type to pathogenesis cannot be determined from these data. Therefore, we specifically depleted either CD4$^+$ or CD8$^+$ T cells from the lungs of mice expressing hDPP4 to determine the relative roles of T cell subtypes in MERS-CoV-mediated disease.

TABLE 4 Pathology scores of lungs of mice depleted of $CD4^+$ T cells and infected with 2.5×10^4 PFU MERS-CoV(Jordan)[a]

	Mean pathology score of animals treated with indicated antibody							
	Mock infection				MERS-CoV infection			
	4 dpi		7 dpi		4 dpi		7 dpi	
Pathological sign	IgG	Anti-CD4	IgG	Anti-CD4	IgG	Anti-CD4	IgG	Anti-CD4
Overall inflammation	+	+	+	+	++	++	++	++
Bronchiolar inflammation	+	+	+	+	++	++	++	++
Perivascular inflammation	+	+	+	+	++	++	++	++
Edema	+	+	+	+	+	+	+	+
Eosinophils	+	+	+	+	++	+	++	+
Neutrophils	+	+	+	+	++	+	+	+
Macrophages	+	+	+	+	++	++	++	++
Lymphocytes	+	+	+	+	++	++	++	++
Pleuritis	+	+	+	+	+	++	+	+
Epithelial necrosis	+	+	+	+	+	+	+	+

[a]Lung sections from 5 MERS-CoV-infected mice per group were scored for pathological signs of disease on a scale of 0 to 5, and scores were averaged and rounded to the nearest whole number: +, 0 or 1; ++, 2 or 3; +++, 4 or 5; dpi, days postinfection.

Depletion of $CD4^+$ T cells resulted in no significant histological changes in MERS-CoV-induced lung pathology at either day 4 or day 7 postinfection (Table 4). There was also no statistically significant effect of $CD4^+$ T cell depletion on the MERS-CoV-dependent weight loss ($P > 0.05$) (Fig. 6A) or on the MERS-CoV titer in the lungs of infected mice at day 4 or 7 postinfection ($P > 0.05$) (Fig. 6B). These data suggest that $CD4^+$ T cells do not contribute to MERS-CoV replication, persistence, or pathogenesis *in vivo*.

In contrast, depleting $CD8^+$ T cells slightly exacerbated MERS-CoV-induced overall inflammation, bronchiolar inflammation, lymphocyte infiltration, and pleuritis at day 7 postinfection (Table 5), as assessed by histology. No significant changes in lung pathology were observed at day 4 postinfection. Interestingly, despite the mildly worse inflammation observed at day 7, depletion of $CD8^+$ T cells significantly protected against MERS-CoV-dependent weight loss at days 6 and 7 postinfection (Fig. 6C, squares). For example, at day 7 postinfection MERS-infected mice treated with control antibody dropped to 83.5% $\pm$ 0.75% of their starting weight, whereas $CD8^+$ T cell-depleted mice were at 93.5% $\pm$ 2.1% of starting weight ($P < 0.001$). Depletion of $CD8^+$ T cells had no significant effect on the MERS-CoV titer in the lungs of infected mice at day 4 or 7 postinfection ($P > 0.05$) (Fig. 6D). These data suggest that $CD8^+$ T cells contribute to MERS-CoV-induced lung pathology but do not contribute to the replication, persistence, or control of MERS-CoV *in vivo*.

Depletion of macrophages causes enhanced MERS-CoV-induced weight loss and pathology but does not alter MERS-CoV replication or persistence in infected mice. The data suggest that MERS-CoV disease induces infiltration of macrophages into the lungs of infected mice and also an increase in macrophage activation. We determined the role of macrophages in MERS-CoV infection in hDPP4-expressing mice by depleting macrophages from the lungs of mice using clodronate-containing liposomes.

Depletion of macrophages resulted in no significant changes in pathology at 4 days postinfection compared to treatment with control (phosphate-buffered saline [PBS]) liposomes, except for slightly increased lymphocyte infiltration (Table 6). However, depletion of macrophages did appear to make MERS-CoV-induced overall inflammation, perivascular inflammation, edema, eosinophilia, and lymphocyte infiltration worse at day 7 postinfection than in mock-infected control mice (Table 6). Furthermore, depletion of macrophages from the lungs of hDPP4 mice caused significantly greater weight loss at days 6 and 7 postinfection than in controls (Fig. 6E, squares). For example, at day 7 postinfection, MERS-CoV-infected mice treated with PBS-containing liposomes were at 86.8% $\pm$ 1.2% of starting weight, whereas mice treated with

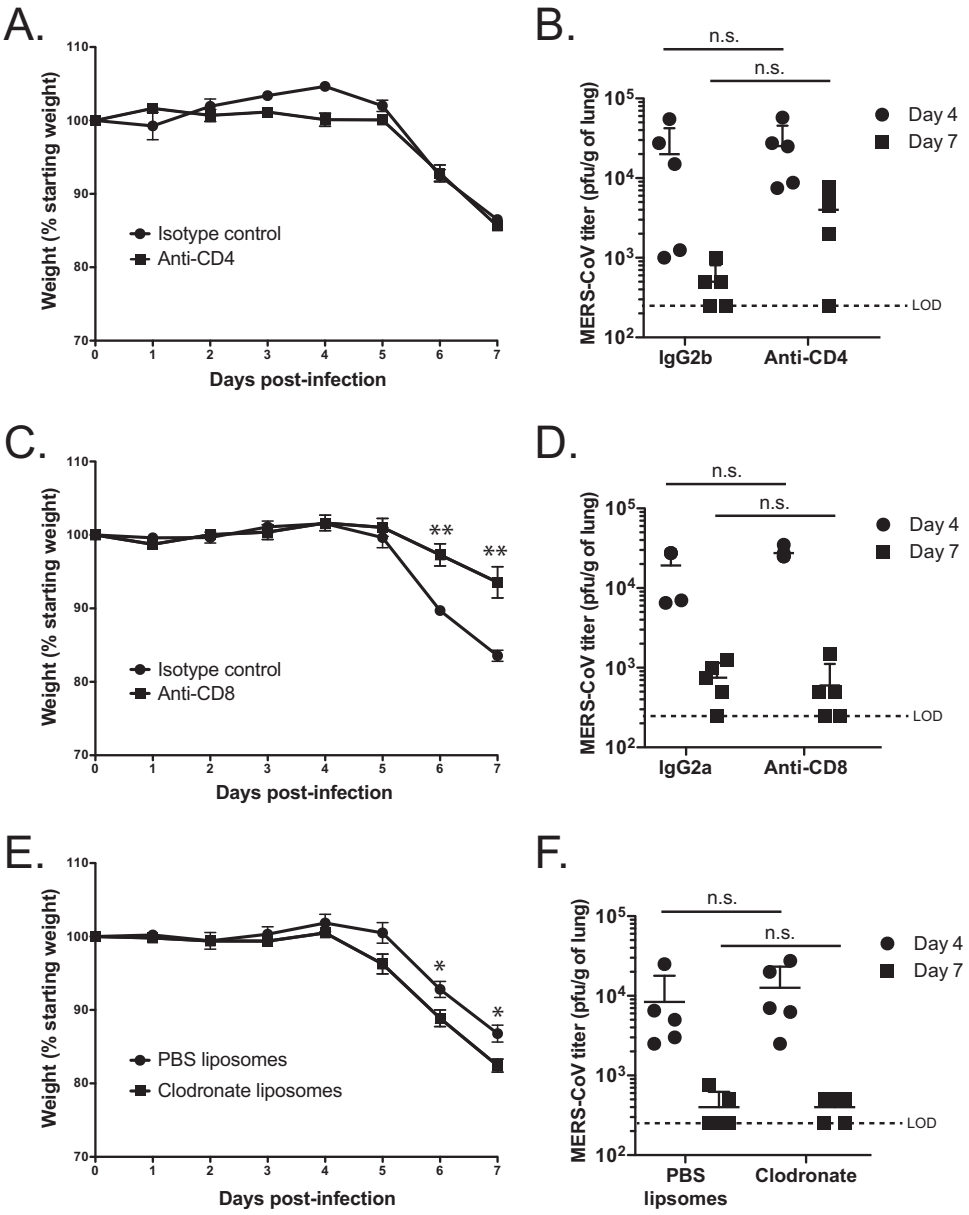

FIG 6 Depletion of CD4$^+$ T cells, CD8$^+$ T cells, or macrophages has differential effects on MERS-CoV pathogenesis in C57B6/hDPP4 mice. C57B6/hDPP4 mice were depleted of CD4$^+$ T cells (A, B), CD8$^+$ T cells (C, D), or macrophages (E, F) and infected with 2.5×10^4 PFU MERS-CoV (Jordan) and monitored for weight loss (A, C, E) and MERS-CoV titer (B, D, F). Data shown are means ± SD for samples, with each of the 5 mice per time point shown as individual dots on the graph in panels B, D, and F. **, $P < 0.01$; *, $P < 0.05$, n.s., not statistically significant. LOD, limit of detection.

clodronate-containing liposomes were at 82% ± 0.9% of starting weight ($P < 0.05$). As we observed with T cells, macrophage depletion had no significant effect on MERS-CoV titers in the lungs of infected mice at day 4 or 7 postinfection (Fig. 6F) ($P > 0.05$). These data suggest that macrophages protect mice from MERS-CoV-dependent lung inflammation but do not promote or inhibit MERS-CoV replication *in vivo*.

DISCUSSION

MERS-CoV is an emerging highly pathogenic coronavirus for which there are no approved treatments or vaccination strategies. In order to develop novel MERS-CoV therapeutics, a well-characterized small-animal model that reproduces the disease seen in humans is required for the early-stage testing of putative therapies *in vivo*. In this

TABLE 5 Pathology scores of lungs of mice depleted of $CD8^+$ T cells and infected with 2.5×10^4 PFU MERS-CoV(Jordan)[a]

	Mean pathology score of animals treated with indicated antibody							
	Mock infection				MERS-CoV infection			
	4 dpi		7 dpi		4 dpi		7 dpi	
Pathological sign	IgG	Anti-CD8	IgG	Anti-CD8	IgG	Anti-CD8	IgG	Anti-CD8
Overall inflammation	+	+	+	+	++	++	++	+++
Bronchiolar inflammation	+	+	+	+	++	++	+	++
Perivascular inflammation	+	+	+	+	++	++	++	++
Edema	+	+	+	+	+	+	+	+
Eosinophils	+	+	+	+	++	++	+	+
Neutrophils	+	+	+	+	++	++	+	+
Macrophages	+	+	+	+	++	++	++	++
Lymphocytes	+	+	+	+	++	++	++	+++
Pleuritis	+	+	+	+	++	++	+	++
Epithelial necrosis	+	+	+	+	+	+	+	+

[a]Lung sections from 5 MERS-CoV-infected mice per group were scored for pathological signs of disease on a scale of 0 to 5, and scores were averaged and rounded to the nearest whole number: +, 0 or 1; ++, 2 or 3; +++, 4 or 5; dpi, days postinfection.

study, we further characterize a mouse model of MERS-CoV that we have previously used to test a novel MERS-CoV therapeutic strategy (27).

Histology data from a MERS-CoV-infected human patient demonstrated that infection is manifested by severe inflammatory lung pathology (10). Previously described mouse models for MERS-CoV infection do not exhibit these traits and thus do not accurately reflect human disease. Here we showed that in humanized mice, hDPP4 expression by organ and immune cell type was equivalent to endogenous mDPP4 expression. Further, we show that infection of hDPP4-expressing mice with different doses of MERS-CoV yields three different disease phenotypes: 2.5×10^4 PFU MERS-CoV causes a 20% weight loss from day 5 to day 7 postinfection; 2.5×10^3 PFU MERS-CoV causes a 10% weight loss by day 7 postinfection, from which the mice recover; and 2.5×10^2 PFU MERS-CoV has no effect on the weight of mice. This is despite the finding that infectious MERS-CoV and MERS-CoV RNA can be recovered from the lungs of mice infected with all three doses, though levels depend on the inoculated dose. All infected mice were clear, or almost clear, of infectious MERS-CoV in the lungs by day 7 postinfection. Interestingly, in mice that survived past 7 days postinfection, MERS-CoV mRNA was still detectable at 21 days postinfection, albeit at much lower levels than at the peak of infection, and there was no evidence of MERS-CoV genomic RNA in the lungs of infected mice at this time point. We hypothesize that the detection of

TABLE 6 Pathology scores of lungs of mice depleted of macrophages and infected with 2.5×10^4 PFU MERS-CoV(Jordan)[a]

	Mean pathology score of animals subjected to indicated liposome treatment							
	Mock infection				MERS-CoV infection			
	4 dpi		7 dpi		4 dpi		7 dpi	
Pathological sign	PBS	Clodronate	PBS	Clodronate	PBS	Clodronate	PBS	Clodronate
Overall inflammation	++	+	+	++	+++	+++	++	+++
Bronchiolar inflammation	+	+	+	+	++	++	+	+
Perivascular inflammation	++	+	+	++	+++	+++	++	+++
Edema	+	+	+	+	+	++	+	++
Eosinophils	++	+	+	+	++	++	+	++
Neutrophils	+	+	+	+	++	++	+	+
Macrophages	++	+	+	+	++	++	++	++
Lymphocytes	+	+	+	++	++	+++	++	+++
Pleuritis	+	+	+	+	++	++	+	+
Epithelial necrosis	+	+	+	+	+	+	+	+

[a]Lung sections from 5 MERS-CoV-infected mice per group were scored for pathological signs of disease on a scale of 0 to 5, and scores were averaged and rounded to the nearest whole number: +, 0 or 1; ++, 2 or 3; +++, 4 or 5; dpi, days postinfection.

MERS-CoV mRNA at this late time point is due to either inherent differences in levels of detection by plaque assays and by qPCR or to the fact that there is a substantial presence of viral RNA that is maintained in a cell population in the lungs after the virus is cleared. Whether this RNA is able to produce live virus at extended time points or potentially under immune cell depletion conditions is unknown. Experiments comparing viral RNA levels and depletion experiments during longer infection times will be analyzed in the future.

Studies have shown that MERS-CoV is capable of spreading to other organs in infected mice when DPP4 is expressed under a strong ubiquitous promoter (23, 25). The recent human case report suggests that MERS-CoV does not spread to any other organ during human infection (10), and we could find no evidence of MERS-CoV spread to the brain, kidney, or liver in C57B6/hDPP4 mice that were exposed to our highest dose of MERS-CoV and succumbed to fatal infection. We detected small amounts of MERS-CoV RNA in the blood and spleen of infected mice, suggesting that MERS-CoV is present in the blood or a circulating cell, such as T cells (6), but the clinical significance of this is unclear. There are only minimal data for the blood titer or immune cell infections *in vivo* in human infections. We hypothesize that the immune cell component of MERS-CoV pathogenesis may provide legitimate models of infection *in vivo*, for example, in circulating T cells. Without additional human MERS-CoV data, it is difficult to know for certain; however, the role of the immune cell component in MERS-CoV pathogenesis and replication is an active area of research in the B6/hDPP4 mouse model.

Histological analysis of the lungs of MERS-CoV-infected hDPP4 mice reveals that MERS-CoV causes significant edema, vascular cuffing, and alveolar septum thickening caused by lymphocyte infiltration. This recapitulates the basic pathology observed in human lungs after severe MERS-CoV infection (10). The decrease in angiogenesis-related and endothelial marker gene expression in our RNA-Seq data is also consistent with the vascular damage observed in the human autopsy study (10). Although the autopsy of this patient describes only cardiac fibrosis, our data show transcriptional changes consistent with fibrosis in the lung, as collagens, Timp1, and transforming growth factor β (TGF-β) are upregulated, and the set of infection-induced gene changes shows strong concordance with those seen in bleomycin-induced fibrosis models.

We have also analyzed infiltrating cell populations by flow cytometry and found significant infiltration of $CD4^+$ T cells, $CD8^+$ T cells, macrophages, and neutrophils into the lungs over the time course of MERS-CoV infection of our hDPP4 mice. RNA-Seq identified a significant transcriptional upregulation of T cell chemokines, such as Cxcl10 and Ccl12, of T cell-associated factors, such as Ccl1, and of factors produced by macrophages, such as Ccl3 and Ccl4. The cellular sources of these cytokine and chemokine transcripts are under investigation, but in light of previous studies (7, 8), macrophages may be a significant source of inflammatory cytokines and chemokines during MERS-CoV infection, regardless of whether they do (8) or do not (7) facilitate productive MERS-CoV replication. The role of macrophages and monocytes in human disease is unknown due to the minimal clinical data from MERS patients. The analysis of MERS-CoV replication or the role of murine macrophages compared to that of human macrophages in pathogenesis *in vivo* is difficult due to the lack of human samples. However, the B6/hDPP4 mouse model can be used to answer the question of how murine monocytes and macrophages respond to MERS-CoV infection and affect disease. We hypothesize that they play an important role in MERS-CoV lung pathology and in the immune response to infection; however, additional experiments are needed to discern the mechanism by which this occurs.

Taken together, our data suggested a strong T cell and macrophage response in the lungs of MERS-CoV-infected hDPP4 mice, so we depleted mice of T cells and macrophages to determine their roles, if any, in MERS-CoV pathogenesis. We found that $CD4^+$ T cells have no effect on MERS-CoV-induced pathology, replication, or persistence in the lungs of infected mice.

Interestingly, depletion of $CD8^+$ T cells improved the physical symptoms of mice infected with MERS-CoV without inhibiting MERS-CoV replication or reducing the pathological signs of disease in the lungs of infected hDPP4 mice, suggesting that $CD8^+$ T cells may contribute to MERS-CoV-induced weight loss in infected mice. Our data suggest that this is not due to the physical presence of large numbers of $CD8^+$ T cells blocking gas exchange, as pathology scores reveal, if anything, more lymphocytes in the lungs of $CD8^+$ T cell-depleted mice. Previous studies have shown that there is no difference between $CD4^+$ and $CD8^+$ T cells in terms of permissiveness to MERS-CoV infection and that MERS-CoV causes T cell apoptosis in mixed T cell cultures (6). Therefore, we hypothesize that there is a unique response of $CD8^+$ T cells to MERS-CoV infection that is responsible for the physical symptoms of disease. These responses could include the specific timing and sensitivity of $CD8^+$ T cell to apoptosis or the production of a cytokine/chemokine that causes more-systemic inflammatory symptoms.

We found that depletion of macrophages exacerbated the physical symptoms and pathological signs of disease in the lungs of MERS-CoV-infected hDPP4 mice without affecting MERS-CoV replication, suggesting that macrophages protect against MERS-CoV-mediated disease. The mechanism of action is under investigation, but one possibility is that macrophages produce a cytokine/chemokine that protects the lung from excessive inflammation. This is intriguing because previous work on the SARS-CoV demonstrated that macrophages in the lungs of mice were detrimental to lung pathology and clearance of SARS-CoV by inhibiting efficient T cell responses (30). Investigation of the differences between SARS-CoV and MERS-CoV in this context may reveal crucial host responses that determine how macrophages respond differently to these highly pathogenic coronaviruses.

A previous study using the adenovirus transduction of hDPP4 into the lungs of mice suggested that T cells play an important role in the clearance of MERS-CoV (22). In that study, MERS-CoV was not cleared from mice that genetically lack all T cells ($TCRa^{-/-}$) but was cleared at levels similar to those of wild-type mice in mice lacking B cells ($uMT^{-/-}$). We found that antibody-based depletion of $CD4^+$ or $CD8^+$ T cells in adult mice had no significant effect on MERS-CoV titers in the lungs of infected mice, suggesting that in our mouse model with depletion, neither subtype alone plays a significant role in the clearance of MERS-CoV. There are marked differences between these two mouse models that could be responsible for the differences in results. First, the Ad/hDPP4 model transduces hDPP4 into any cells that the adenovirus can infect in the lungs, not necessarily the cells that natively express hDPP4. In addition, the expression levels of hDPP4 in the Ad/hDPP4 model vary from the endogenous hDPP4 levels seen in the B6/hDPP4 mice in this study. The MERS-CoV inoculum may also be responsible for the differences, since the inoculum used in this study was one that caused high levels of infection, lung pathology, and clinical disease, which could be overwhelming to the immune response and mask small differences in MERS-CoV replication that may have a much more significant effect on MERS-CoV when the initial inoculum is lower. Finally, the depletion experiments do not result in a total lack of either T cell-type in the lungs, in contrast to the complete knockout mouse experiments in the study by Zhao et al. (22). Therefore, we cannot rule out that there may be a role for T and B cells in the control of viral load for MERS-CoV that was not observed using our current experimental approaches. Comparisons of viral dose, cell depletions, and background differences between the two models would be informative in the future.

Overall, we have utilized a human DPP4-expressing mouse to create a model of MERS-CoV pathogenesis. In this model, we have demonstrated that $CD8^+$ T cells and macrophages influence the course of MERS-CoV-induced disease. This model will allow for the analysis of how individual inflammatory cell types and host-produced factors regulate MERS-CoV pathogenesis.

MATERIALS AND METHODS

Ethics statement. All mouse experiments were performed at the University of Maryland School of Medicine in accordance with protocols approved by the Institutional Animal Care and Use Committee (IACUC) under protocol number 0115009 and the U.S. Animal Welfare Act.

MERS-CoV, Vero E6 cells, and hDPP4-expressing mice. The Jordan MERS-CoV strain (GenBank accession no. KC776174.1, MERS-CoV-Hu/Jordan-N3/2012) was kindly provided by Kanta Subbarao (National Institutes of Health, Bethesda, MD), Gabriel Defang (Naval Medical Research Unit 3 [NAMRU-3], Cairo, Egypt), Michael Cooper (Armed Forces Health Surveillance Center [AFHSC]), and Emad Mohereb (NAMRU-3). All experiments with live MERS-CoV(Jordan) were performed under biosafety level 3 conditions at the University of Maryland School of Medicine.

Vero E6 cells (monkey kidney epithelial cells, ATCC CRL-1586) for plaque assays were grown in minimal essential media (MEM; Corning) supplemented with 10% (vol/vol) fetal bovine serum (FBS; Sigma-Aldrich), 1% (vol/vol) L-glutamine (Gibco), and 1% (vol/vol) penicillin-streptomycin (Gemini bioproducts) at 37°C in a 5% CO_2 atmosphere.

Human DPP4 (hDPP4)-expressing C57B6 mice (C57B6/hDPP4 mice) were created and provided by Regeneron Pharmaceuticals Inc. as described previously (27). Mice that were heterozygous for hDPP4 were bred at the University of Maryland School of Medicine by crossing hDPP4 homozygotes with mDPP4 homozygotes.

Mouse genotyping and human and mouse DPP4 quantification by TaqMan assay. Eight- to 12-week-old C57/B6 mice were genotyped using the Extract-N-Amp Tissue PCR kit (Sigma-Aldrich) on tail clips according to the manufacturers' instructions. PCR for both mDPP4 and hDPP4 was performed using a common forward primer (CTGGCTTAGATCTCTGGCGT), an mDPP4 reverse primer (ATTGGCACGGTGAT GATGGTG), and an hDPP4 reverse primer (TAAGACGGAGCCTGACCTGA). PCR products were run on a 1% agarose gel and assigned as wild type for mDPP4 expression (hDPP4$^{-/-}$) or as heterozygote (hDPP4$^{+/-}$) or homozygote (hDPP4$^{+/+}$) for hDPP4 expression based on band migration.

Eight- to 12-week-old C57/B6 mice were euthanized using isoflurane (Butler Animal Health Supply), and the following organs were harvested: brain, heart, intestine (small), lung, liver, kidney, and spleen. Blood was obtained by dissection of the aorta in the thoracic cavity, allowing the blood to pool in the thoracic cavity, and removed by pipette.

All organs were homogenized in TRIzol reagent (Ambion) using 1.0-mm glass beads (Sigma-Aldrich) and a MagNA lyser (Roche). RNA was extracted using Direct-zol RNA miniprep (Zymo Research) according to the manufacturer's instructions. Human and mouse DPP4 mRNA expression was quantified using the Fast 1-step PCR mix (Life Technologies) according to the manufacturer's instructions with specific TaqMan gene expression assays for hDPP4 and mDPP4 (Applied Biosystems).

Threshold cycle (C_T) values were assessed and analyzed using a 7500 Fast Dx PCR instrument (Applied Biosystems), and relative DPP4 expression levels were determined using the $\Delta\Delta C_T$ method, comparing to hDPP4$^{+/+}$ for mDPP4 expression and hDPP4$^{-/-}$ for hDPP4 expression.

Mouse infections. Eight- to 12-week-old C57/B6 mice heterozygote for hDPP4 (hDPP4$^{+/-}$) were used in all MERS-CoV infection experiments. Prior to intranasal inoculation, mice were anesthetized by intraperitoneal injection using a mix of xylazine (0.38 mg/mouse) and ketamine (1.3 mg/mouse) diluted in PBS to make a total volume of 50 μl per mouse. Once anesthetized, mice were intranasally inoculated with PBS or 2.5×10^2 PFU, 2.5×10^3 PFU, or 2.5×10^4 PFU of MERS-CoV(Jordan) diluted into PBS for a 50-μl total inoculum. During the experiments, mice were weighed on the day of infection and every day of the experiment to assess MERS-CoV-induced weight loss.

At noted time points postinfection, or when mice reached ≤80% of their starting body weight, mice were euthanized using isoflurane (Butler Animal Health Supply). Lungs and, for some experiments, kidneys, brains, blood, and liver were harvested for analysis of MERS-CoV replication and pathology.

MERS-CoV quantification. For live MERS-CoV titers, organs from infected mice where homogenized in PBS (Quality Biological Inc.) using 1.0-mm glass beads (Sigma-Aldrich) and a beadruptor (Omni International Inc.). MERS-CoV titers in PFU per milliliter were determined by plaque assay as previously described (31) and then converted to PFU/gram of lung based on the mass of the harvested lung.

For MERS-CoV genomic RNA and M mRNA quantification, organs from infected mice were homogenized in TRIzol reagent (Ambion) using 1.0-mm glass beads (Sigma-Aldrich) and a beadruptor (Omni International Inc.). RNA was extracted using the Direct-zol RNA miniprep kit (Zymo Research) according to the manufacturer's instructions. Levels of MERS-CoV genomic RNA and M mRNA were determined using the Fast 1-step PCR mix (Life Technologies) according to the manufacturer's instructions with previously described specific primers and probes targeting UpE for MERS-CoV genomic RNA and the membrane (M) protein mRNA (Life Technologies [31]). Mouse transferrin receptor protein 1 (TFRC) was used as the endogenous control and was detected using the following primers and probe: forward primer, ATGACGTTGAATTGAACCTGGACTA; reverse primer, GTCTCCACGAGCGGAATACAG; probe, ABY-A TCAGGGATATGGGTCTAAGTCTACAGTGG-QSY. C_T values were determined using a 7500 Fast Dx PCR instrument (Applied Biosystems), and relative MERS-CoV mRNA expression levels were determined using the $\Delta\Delta C_T$ method with comparison to mock-infected controls. All $\Delta\Delta C_T$ values of <1 were corrected to equal 1.

Histology. Paraformaldehyde-fixed lungs were embedded in paraffin and sectioned before hematoxylin and eosin (H&E) staining by the Pathology Electron Microscopy and Histology Laboratory at the University of Maryland School of Medicine. Slides were blindly scored for pathological signs of disease on a scale of 0 to 5 by Sarah Beck at the Department of Molecular and Comparative Pathobiology, Johns Hopkins School of Medicine. Scored categories are for bronchiolar inflammation, perivascular inflammation, edema, eosinophils, neutrophils, macrophages, lymphocytes, pleuritis, and epithelial necrosis. The

overall inflammation score is based on bronchiolar inflammation, perivascular inflammation, and interstitial inflammatory response. Scores were then averaged, rounded to the nearest whole number, and then assigned a rating as low/none (0 or 1; indicated as +), medium (2 or 3; ++), or high (4 or 5; +++).

Inflammatory cytokine and receptor PCR arrays. Levels of expression of inflammatory cytokines and receptors were assessed using the mouse inflammatory cytokines and receptors RT² profiler PCR array (Qiagen) according to the manufacturer's instructions. C_T values in reactions were assessed using a 7500 Fast Dx PCR instrument (Applied Biosystems) and analyzed using RT² profiler PCR array online analysis software (SABiosciences).

Flow cytometry. hDPP4-expressing mice were infected with 2.5×10^4 PFU MERS-CoV(Jordan), and lungs were harvested for flow cytometry at 2, 4, and 7 days postinfection. Lungs from infected mice were dissociated using a mouse lung dissociation kit, gentleMACS tubes, and the gentleMACS dissociator (all from Miltenyi Biotec) according to the manufacturer's instructions. Red blood cells were removed using ammonium-chloride-potassium lysis buffer (ACK; Quality Biological) according to the manufacturer's instructions. Cells were then washed once in flow cytometry buffer (PBS supplemented with 2% FBS, 0.1% sodium azide, and 2 mM EDTA) and resuspended in F_c blocking buffer (flow cytometry buffer containing Mouse Fc Block [Beckton Dickinson]). Following one wash in flow cytometry buffer, cells were stained with antibodies to CD3ε (clone number 145-2C11; BioLegend), CD4 (clone number GK1.1; BD Biosciences), CD8α (clone number 53-6.7; BD Pharmingen), CD11b (clone number M1/70; BioLegend), CD11c (clone number N418; Tonbo Biosciences), CD19 (clone number 6D5; BioLegend), CD45R (B220; clone number RA3-6B2; BD Pharmingen), CD49b (clone number DX5; BioLegend), F4/80 (clone number BM8; BioLegend), major histocompatibility complex class II (MHC-II; clone number M5/114.15.2; BioLegend), CD193 (clone number J073E5; Biolegend), CD200R3 (clone number Bal3; Biolegend), FcεRIα (clone number MAR-1; Biolegend), Ly6G (clone number RB6-8C5; eBiosciences), or NK1.1 (clone number PK13.6; BD Biosciences). Following staining, cells were fixed in 4% methanol-free paraformaldehyde (Thermo Scientific) overnight and then were pelleted, resuspended in PBS, and analyzed on an LSR II flow cytometer (Beckton Dickinson); data were analyzed using FlowJo analysis software (FlowJo LLC). Splenic cells from mock-infected controls were stained and used to set flow cytometry compensation levels.

Based on staining characteristics, individual cell populations were identified as B cells (CD3ε^- CD19$^+$ B220$^+$), natural killer (NK) cells (CD3ε^- CD49b$^+$ NK1.1$^+$), T cells (CD3ε^+ CD4$^+$ for T helper cells or CD3ε^+ CD8α^+ for cytotoxic T cells), dendritic cells (DCs; CD11c$^+$ MHCII$^+$), macrophages (CD11b$^+$ F4/80$^+$ MHC-II$^+$), basophils (FcεRIα^+ CD200R3$^+$), eosinophils (F4/80$^+$ CD193$^+$), or neutrophils (CD11b$^+$ Ly6G$^+$).

Splenocytes from hDPP4$^{-/-}$, hDPP4$^{+/-}$, or hDPP4$^{+/+}$ mice were stained for DPP4 using antibodies to mDPP4 (clone number 155202; R&D Systems) and hDPP4 (clone number 2A6; eBiosciences). DPP4 staining was assessed using an Amnis Flowsight Imaging flow cytometer (Millipore).

Immune cell depletions. T helper cells and cytotoxic T cells were depleted from mice by intraperitoneal (i.p.) injection of 100 μl of PBS containing 30 μg CD4 antibody (rat IgG2b clone number GK1.5; eBiosciences) or 40 μg CD8α antibody (rat IgG2a clone number 53-6.7; eBiosciences), respectively, or with PBS containing 40 μg IgG2a (clone number eBR2a; eBiosciences) or 30 μg IgG2b (clone number eB149/10H5; eBiosciences) isotype controls (32).

Macrophages were depleted from the lungs of mice using liposomes containing clodronate (33). Mice were anesthetized by intraperitoneal injection using a mixture of xylazine (0.38 mg/mouse) and ketamine (1.3 mg/mouse) diluted in PBS to make a total volume of 50 μl per mouse. Once anesthetized, mice were intranasally inoculated with 50 μl of PBS or clodronate-containing liposomes (both from ClodronateLiposomes).

We achieved a specific $\geq$90% reduction in splenic CD4$^+$ or CD8$^+$ T cells and a $\geq$75% reduction of lung macrophages, with no reduction in lung dendritic cells, out to 3 days posttreatment. Therefore, mice were depleted of T cells, macrophages, or relevant controls at day 1 preinfection, day 2 postinfection, and day 5 postinfection in order to maintain the depletions for the whole time course of infection.

Mice were infected with 2.5×10^4 PFU MERS-CoV(Jordan) and monitored for weight loss. Lungs were harvested at day 4 or day 7 postinfection for histology, titer by plaque assay, or RNA extraction.

RNA preparation, RNA sequencing read mapping, and differential expression analysis. C57B6/hDPP4 mice were inoculated with 2.5×10^4 PFU of MERS-CoV(Jordan) or PBS, and lungs were harvested at days 2, 4, or 7 postinfection. Total RNA was purified using the MagMAX-96 for Microarrays Total RNA Isolation kit (Ambion) according to the manufacturer's instructions, in which genomic DNA was removed using MagMAXTurboDNase buffer and Turbo DNase. mRNA was purified from total RNA using the Dynabeads mRNA purification kit (Invitrogen) according to the manufacturer's instructions. Strand-specific RNA sequencing (RNA-Seq) libraries were prepared using the ScriptSeq mRNA-Seq Library Preparation kit (Epicentre). Twelve-cycle PCR was performed to amplify libraries. Sequencing was performed on an Illumina HiSeq2000 instrument by a multiplexed, single-read run with 33 cycles. Raw sequence data (BCL files) were converted to Fastq format via Illumina Casava 1.8.2. Reads were decoded based on their barcodes, and read quality was evaluated using Fastqc (www.bioinformatics.babraham.ac.uk/projects/fastqc/). Reads were mapped to the mouse transcriptome (GRCm38 with NCBI annotation release 104), and reads mapping to sense strand exons were summed at the gene level using the RNA-Seq workflow of CLC Genomics Server version 6.0 (Qiagen) as described previously (34).

Genes differentially expressed between MERS-CoV-infected and mock-infected lungs were obtained using DeSeq 1.6 (35). A gene was considered regulated in a particular comparison if the *P* value from DeSeq was less than 0.01 and if the mean expression increased or decreased by at least 50%. For the latter, means were calculated after upper quartile normalization of the raw gene counts. The set of all genes regulated this way is termed a gene expression signature and is used in NextBio analysis.

Statistics. Data for TaqMan assays, MERS-CoV quantitation, and flow cytometry analyses are presented as means ± standard errors of the means (SEM) and were analyzed using a Student *t* test or two-way analysis of variance (ANOVA) with a Bonferroni posttest, as appropriate. Statistical significance was obtained when *P* values were <0.05.

SUPPLEMENTAL MATERIAL

Supplemental material for this article may be found at https://doi.org/10.1128/JVI.01825-16.

DATASET S1, XLS file, 1.0 MB.

DATASET S2, XLS file, 0.07 MB.

ACKNOWLEDGMENTS

This work was supported in part by NIH grant R01 AI095569 to M.B.F., NIH grant T32 AI095190 to T.V., NIH grant F32 AI118303 to J.M.S., NIH grant R01 HL127422 to S.R., and Regeneron Pharmaceuticals.

We thank the members of the Frieman lab for their help in preparing the manuscript.

REFERENCES

1. Zaki AM, van Boheemen S, Bestebroer TM, Osterhaus AD, Fouchier RA. 2012. Isolation of a novel coronavirus from a man with pneumonia in Saudi Arabia. N Engl J Med 367:1814–1820. https://doi.org/10.1056/NEJMoa1211721.
2. Lee SS, Wong NS. 2015. Probable transmission chains of Middle East respiratory syndrome coronavirus and the multiple generations of secondary infection in South Korea. Int J Infect Dis 38:65–67. https://doi.org/10.1016/j.ijid.2015.07.014.
3. Ki M. 2015. 2015 MERS outbreak in Korea: hospital-to-hospital transmission. Epidemiol Health 37:e2015033. https://doi.org/10.4178/epih/e2015033.
4. Raj VS, Mou H, Smits SL, Dekkers DH, Muller MA, Dijkman R, Muth D, Demmers JA, Zaki A, Fouchier RA, Thiel V, Drosten C, Rottier PJ, Osterhaus AD, Bosch BJ, Haagmans BL. 2013. Dipeptidyl peptidase 4 is a functional receptor for the emerging human coronavirus-EMC. Nature 495:251–254. https://doi.org/10.1038/nature12005.
5. Zhong J, Rao X, Rajagopalan S. 2013. An emerging role of dipeptidyl peptidase 4 (DPP4) beyond glucose control: potential implications in cardiovascular disease. Atherosclerosis 226:305–314. https://doi.org/10.1016/j.atherosclerosis.2012.09.012.
6. Chu H, Zhou J, Wong BH, Li C, Chan JF, Cheng ZS, Yang D, Wang D, Lee AC, Li C, Yeung ML, Cai JP, Chan IH, Ho WK, To KK, Zheng BJ, Yao Y, Qin C, Yuen KY. 2016. Middle East respiratory syndrome coronavirus efficiently infects human primary T lymphocytes and activates the extrinsic and intrinsic apoptosis pathways. J Infect Dis 213:904–914. https://doi.org/10.1093/infdis/jiv380.
7. Tynell J, Westenius V, Ronkko E, Munster VJ, Melen K, Osterlund P, Julkunen I. 2016. Middle East respiratory syndrome coronavirus shows poor replication but significant induction of antiviral responses in human monocyte-derived macrophages and dendritic cells. J Gen Virol 97:344–355. https://doi.org/10.1099/jgv.0.000351.
8. Zhou J, Chu H, Li C, Wong BH, Cheng ZS, Poon VK, Sun T, Lau CC, Wong KK, Chan JY, Chan JF, To KK, Chan KH, Zheng BJ, Yuen KY. 2014. Active replication of Middle East respiratory syndrome coronavirus and aberrant induction of inflammatory cytokines and chemokines in human macrophages: implications for pathogenesis. J Infect Dis 209:1331–1342. https://doi.org/10.1093/infdis/jit504.
9. Karin N, Wildbaum G. 2015. The role of chemokines in shaping the balance between CD4(+) T cell subsets and its therapeutic implications in autoimmune and cancer diseases. Front Immunol 6:609. https://doi.org/10.3389/fimmu.2015.00609.
10. Ng DL, Al Hosani F, Keating MK, Gerber SI, Jones TL, Metcalfe MG, Tong S, Tao Y, Alami NN, Haynes LM, Mutei MA, Abdel-Wareth L, Uyeki TM, Swerdlow DL, Barakat M, Zaki SR. 2016. Clinicopathologic, immunohistochemical, and ultrastructural findings of a fatal case of Middle East respiratory syndrome coronavirus infection in the United Arab Emirates, April 2014. Am J Pathol 186:652–658. https://doi.org/10.1016/j.ajpath.2015.10.024.
11. de Wit E, Rasmussen AL, Falzarano D, Bushmaker T, Feldmann F, Brining DL, Fischer ER, Martellaro C, Okumura A, Chang J, Scott D, Benecke AG, Katze MG, Feldmann H, Munster VJ. 2013. Middle East respiratory syndrome coronavirus (MERS-CoV) causes transient lower respiratory tract infection in rhesus macaques. Proc Natl Acad Sci U S A 110:16598–16603. https://doi.org/10.1073/pnas.1310744110.
12. Munster VJ, de Wit E, Feldmann H. 2013. Pneumonia from human coronavirus in a macaque model. N Engl J Med 368:1560–1562. https://doi.org/10.1056/NEJMc1215691.
13. Yao Y, Bao L, Deng W, Xu L, Li F, Lv Q, Yu P, Chen T, Xu Y, Zhu H, Yuan J, Gu S, Wei Q, Chen H, Yuen KY, Qin C. 2014. An animal model of MERS produced by infection of rhesus macaques with MERS coronavirus. J Infect Dis 209:236–242. https://doi.org/10.1093/infdis/jit590.
14. Falzarano D, de Wit E, Feldmann F, Rasmussen AL, Okumura A, Peng X, Thomas MJ, van Doremalen N, Haddock E, Nagy L, LaCasse R, Liu T, Zhu J, McLellan JS, Scott DP, Katze MG, Feldmann H, Munster VJ. 2014. Infection with MERS-CoV causes lethal pneumonia in the common marmoset. PLoS Pathog 10:e1004250. https://doi.org/10.1371/journal.ppat.1004250.
15. Johnson RF, Via LE, Kumar MR, Cornish JP, Yellayi S, Huzella L, Postnikova E, Oberlander N, Bartos C, Ork BL, Mazur S, Allan C, Holbrook MR, Solomon J, Johnson JC, Pickel J, Hensley LE, Jahrling PB. 2015. Intratracheal exposure of common marmosets to MERS-CoV Jordan-n3/2012 or MERS-CoV EMC/2012 isolates does not result in lethal disease. Virology 485:422–430. https://doi.org/10.1016/j.virol.2015.07.013.
16. Wentworth DE, Gillim-Ross L, Espina N, Bernard KA. 2004. Mice susceptible to SARS coronavirus. Emerg Infect Dis 10:1293–1296. https://doi.org/10.3201/eid1007.031119.
17. Roberts A, Deming D, Paddock CD, Cheng A, Yount B, Vogel L, Herman BD, Sheahan T, Heise M, Genrich GL, Zaki SR, Baric R, Subbarao K. 2007. A mouse-adapted SARS-coronavirus causes disease and mortality in BALB/c mice. PLoS Pathog 3:e5. https://doi.org/10.1371/journal.ppat.0030005.
18. Coleman CM, Matthews KL, Goicochea L, Frieman MB. 2014. Wild-type and innate immune-deficient mice are not susceptible to the Middle East respiratory syndrome coronavirus. J Gen Virol 95:408–412. https://doi.org/10.1099/vir.0.060640-0.
19. Cockrell AS, Peck KM, Yount BL, Agnihothram SS, Scobey T, Curnes NR, Baric RS, Heise MT. 2014. Mouse dipeptidyl peptidase 4 is not a functional receptor for Middle East respiratory syndrome coronavirus infection. J Virol 88:5195–5199. https://doi.org/10.1128/JVI.03764-13.
20. van Doremalen N, Miazgowicz KL, Milne-Price S, Bushmaker T, Robertson S, Scott D, Kinne J, McLellan JS, Zhu J, Munster VJ. 2014. Host species restriction of Middle East respiratory syndrome coronavirus through its receptor, dipeptidyl peptidase 4. J Virol 88:9220–9232. https://doi.org/10.1128/JVI.00676-14.
21. Peck KM, Cockrell AS, Yount BL, Scobey T, Baric RS, Heise MT. 2015. Glycosylation of mouse DPP4 plays a role in inhibiting Middle East respiratory syndrome coronavirus infection. J Virol 89:4696–4699. https://doi.org/10.1128/JVI.03445-14.

22. Zhao J, Li K, Wohlford-Lenane C, Agnihothram SS, Fett C, Gale MJ, Jr, Baric RS, Enjuanes L, Gallagher T, McCray PB, Jr, Perlman S. 2014. Rapid generation of a mouse model for Middle East respiratory syndrome. Proc Natl Acad Sci U S A 111:4970–4975. https://doi.org/10.1073/pnas.1323279111.
23. Agrawal AS, Garron T, Tao X, Peng BH, Wakamiya M, Chan TS, Couch RB, Tseng CT. 2015. Generation of a transgenic mouse model of Middle East respiratory syndrome coronavirus infection and disease. J Virol 89:3659–3670. https://doi.org/10.1128/JVI.03427-14.
24. Gorrell MD, Gysbers V, McCaughan GW. 2001. CD26: a multifunctional integral membrane and secreted protein of activated lymphocytes. Scand J Immunol 54:249–264. https://doi.org/10.1046/j.1365-3083.2001.00984.x.
25. Tao X, Garron T, Agrawal AS, Algaissi A, Peng BH, Wakamiya M, Chan TS, Lu L, Du L, Jiang S, Couch RB, Tseng CT. 2015. Characterization and demonstration of the value of a lethal mouse model of Middle East respiratory syndrome coronavirus infection and disease. J Virol 90:57–67. https://doi.org/10.1128/JVI.02009-15.
26. Li K, Wohlford-Lenane C, Perlman S, Zhao J, Jewell AK, Reznikov LR, Gibson-Corley KN, Meyerholz DK, McCray PB, Jr. 2016. Middle East respiratory syndrome coronavirus causes multiple organ damage and lethal disease in mice transgenic for human dipeptidyl peptidase 4. J Infect Dis 213:712–722. https://doi.org/10.1093/infdis/jiv499.
27. Pascal KE, Coleman CM, Mujica AO, Kamat V, Badithe A, Fairhurst J, Hunt C, Strein J, Berrebi A, Sisk JM, Matthews KL, Babb R, Chen G, Lai KM, Huang TT, Olson W, Yancopoulos GD, Stahl N, Frieman MB, Kyratsous CA. 2015. Pre- and postexposure efficacy of fully human antibodies against Spike protein in a novel humanized mouse model of MERS-CoV infection. Proc Natl Acad Sci U S A 112:8738–8743. https://doi.org/10.1073/pnas.1510830112.
28. Heng TS, Painter MW, Immunological Genome Project Consortium. 2008. The Immunological Genome Project: networks of gene expression in immune cells. Nat Immunol 9:1091–1094. https://doi.org/10.1038/ni1008-1091.
29. Kupershmidt I, Su QJ, Grewal A, Sundaresh S, Halperin I, Flynn J, Shekar M, Wang H, Park J, Cui W, Wall GD, Wisotzkey R, Alag S, Akhtari S, Ronaghi M. 2010. Ontology-based meta-analysis of global collections of high-throughput public data. PLoS One 55(9):e13066. https://doi.org/10.1371/journal.pone.0013066.
30. Zhao J, Van Rooijen N, Perlman S. 2009. Evasion by stealth: inefficient immune activation underlies poor T cell response and severe disease in SARS-CoV-infected mice. PLoS Pathog 5:e1000636. https://doi.org/10.1371/journal.ppat.1000636.
31. Coleman CM, Frieman MB. 2015. Growth and quantification of MERS-CoV infection. Curr Protoc Microbiol 37:15E.2.1-9. https://doi.org/10.1002/9780471729259.mc15e02s37.
32. Loubaki L, Tremblay T, Bazin R. 2013. In vivo depletion of leukocytes and platelets following injection of T cell-specific antibodies into mice. J Immunol Methods 393:38–44. https://doi.org/10.1016/j.jim.2013.04.004.
33. Van Rooijen N, Sanders A. 1994. Liposome mediated depletion of macrophages: mechanism of action, preparation of liposomes and applications. J Immunol Methods 174:83–93. https://doi.org/10.1016/0022-1759(94)90012-4.
34. Mortazavi A, Williams BA, McCue K, Schaeffer L, Wold B. 2008. Mapping and quantifying mammalian transcriptomes by RNA-Seq. Nat Methods 5:621–628. https://doi.org/10.1038/nmeth.1226.
35. Anders S, Huber W. 2010. Differential expression analysis for sequence count data. Genome Biol 11:R106. https://doi.org/10.1186/gb-2010-11-10-r106.